

Effects of droplet size and perfluorocarbon boiling point on the frequency dependence of acoustic vaporization threshold

Mitra Aliabouzar, Krishna N Kumar, and Kausik Sarkar

Citation: [The Journal of the Acoustical Society of America](#) **145**, 1105 (2019); doi: 10.1121/1.5091781

View online: <https://doi.org/10.1121/1.5091781>

View Table of Contents: <https://asa.scitation.org/toc/jas/145/2>

Published by the [Acoustical Society of America](#)

Effects of droplet size and perfluorocarbon boiling point on the frequency dependence of acoustic vaporization threshold

Mitra Aliabouzar, Krishna N Kumar, and Kausik Sarkar^{a)}

Department of Mechanical and Aerospace Engineering, The George Washington University, Washington, DC 20052, USA

(Received 10 December 2018; revised 30 January 2019; accepted 4 February 2019; published online 28 February 2019)

Phase shift liquid perfluorocarbon (PFC) droplets vaporizable by ultrasound into echogenic microbubble above a threshold pressure, termed acoustic droplet vaporization (ADV), are used for therapeutic and diagnostic applications. This study systematically investigated the effect of excitation frequency (2.25, 10, and 15 MHz) on the ADV and inertial cavitation (IC) thresholds of lipid-coated PFC droplets of three different liquid cores—perfluoropentane (PFP), perfluorohexane (PFH), and perfluorooctyl bromide (PFOB)—and of two different sizes—average diameters smaller than 3 μm and larger than 10 μm —in a tubeless setup. This study found that the ADV threshold increases with frequency for the lowest boiling point liquid, PFP, for both large and small size droplets. For higher boiling point liquids, PFH and PFOB, this study did not detect vaporization for small size droplets at the excitation levels (maximum 4 MPa peak negative) studied here. The large PFOB droplets experienced ADV only at the highest excitation frequency 15 MHz. For large PFH droplets, ADV threshold decreases with frequency that could possibly be due to the superharmonic focusing being a significant effect at larger sizes and the higher excitation pressures. ADV thresholds at all the frequencies studied here occurred at lower rarefactional pressures than IC thresholds indicating that phase transition precedes inertial cavitation. © 2019 Acoustical Society of America.

<https://doi.org/10.1121/1.5091781>

[CCC]

Pages: 1105–1116

I. INTRODUCTION

Current commercially available microbubbles (MBs) are limited to micrometer size range and have relatively short *in vivo* half-life due to premature dissolution (Katiyar *et al.*, 2009; Sarkar *et al.*, 2009; Sheeran *et al.*, 2013). The micrometer size distribution restricts them to the vascular space and therefore they cannot be used for extravascular interrogations (Ferrara *et al.*, 2007). Production of MBs in submicrometer range is challenging and would respond poorly to ultrasound stimulation within the diagnostic range. To mitigate these limitations, researchers are investigating clinical potentials of emulsions of phase shift micro- and nanodroplets of volatile perfluorocarbon liquids (PFC) that can be vaporized *in situ* into highly echogenic microbubbles by external application of ultrasound pulses (Kripfgans *et al.*, 2000; Fabiilli *et al.*, 2009; Reznik *et al.*, 2011; Sheeran *et al.*, 2013; Aliabouzar *et al.*, 2018). The vaporization of the liquid core using acoustic waves, termed acoustic droplet vaporization (ADV), occurs beyond a threshold peak negative pressure. We have recently determined the ADV threshold of an emulsion of perfluoropentane (PFP) droplets as a function of frequency by investigating the scattered responses from the system (Aliabouzar *et al.*, 2018). Here, we extend the investigation to systems with different droplet

cores and sizes, determining their ADV as well as inertial cavitation (IC) thresholds, varying the excitation frequency.

Since the pioneering study of Kripfgans *et al.* (2000), the ADV of liquid PFC droplets has been investigated for many diagnostic and therapeutic applications (Fabiilli *et al.*, 2010; Kopechek *et al.*, 2013; Zhang *et al.*, 2013; Vlasisavljevich *et al.*, 2015). The ADV threshold has been determined acoustically as well as by direct optical observation of vaporization using high speed cameras. A review of the past studies using both techniques has been provided in our previous paper (Aliabouzar *et al.*, 2018). As noted there, ADV thresholds obtained in different studies cannot be directly compared due to differences in the setups, droplet size distribution, and the method of threshold determination. However, some trends have been found to be consistent across experiments, e.g., the ADV threshold decreases with increasing droplet size (Kripfgans *et al.*, 2004; Fabiilli *et al.*, 2009; Schad and Hynnen, 2010; Sheeran *et al.*, 2011), increasing temperature (Zhang and Porter, 2010; Reznik *et al.*, 2011), and increasing number of cycles (Lo *et al.*, 2007; Reznik *et al.*, 2011). However, ADV threshold showed an increasing trend with increasing excitation frequency when observed by optical means (Kripfgans *et al.*, 2002; Kripfgans *et al.*, 2004; Sheeran *et al.*, 2013) and an opposite decreasing trend when determined by echogenicity-based techniques (Kripfgans *et al.*, 2000; Schad and Hynnen, 2010; Williams *et al.*, 2013). In our previous article, we noted that the contradictory results obtained in the literature have been ascribed by their authors to limitations of the optical setup (Kripfgans *et al.*, 2004) as well as insufficient distinction between IC and

^{a)}Present address: The George Washington University, 800 22nd Street North West, Suite 3000, Washington, DC 20052, USA. Electronic mail: sarkar@gwu.edu

ADV; experimentally measured IC threshold always increased with excitation frequency, the reason being the longer continuous duration of negative pressure during the rarefactional half cycle (Apfel and Holland, 1991). We acoustically determined the ADV threshold of a system of PFP droplets in a tubeless setup using scattered (fundamental, sub-, and second harmonic) responses. We found the ADV threshold for our system determined at room temperature to increase with increasing frequency (Aliabouzar *et al.*, 2018). The ADV threshold decreasing with increasing excitation frequency is nominally at odds with classical nucleation theory (CNT), and has been argued to be resulting from heterogeneous nucleation or droplet deformation (Kripfgans *et al.*, 2004) or nonlinear propagation and super-harmonic focusing (Li *et al.*, 2014; Shpak *et al.*, 2014; Miles *et al.*, 2016). However, Shpak *et al.* (2014) noted that super-harmonic focusing was only effective for larger droplets, as for smaller droplets one would need higher frequency of activation, where the attenuation of higher harmonics would also be higher, effectively reducing the nonlinear distortion phenomenon.

Here, we applied our acoustic methodology to droplets of different average sizes and different liquid cores. Droplets of three different PFC liquid cores—perfluoropentane (PFP), perfluorohexane (PFH), and perfluorooctyle bromide (PFOB)—were investigated. The experiments were performed at 37 °C, above the bulk boiling point of PFP, but below those of the PFH and PFOB. For the highest bulk boiling point liquid, PFOB, experiments were also performed at 43 °C. The first objective of this study was to explore the effects of droplet size and the boiling point of PFC liquids on the ADV and IC thresholds. The second objective was to investigate the frequency dependence of the ADV and IC thresholds of emulsions of different liquid cores (different boiling points and surface tensions) and droplet sizes. We used the scattered responses—peak-to-peak, fundamental, sub-, and second harmonic, as well as integrated power spectrum in the low frequency range (500–900 kHz) for estimation of ADV and IC thresholds, respectively.

II. EXPERIMENTAL METHODOLOGY

A. Synthesis and characterization of droplets

In this study, we have used three different PFC liquids: PFP, PFH, and PFOB (99% wt. purity, FluoroMed, Round Rock, TX, USA) as the liquid core. The properties of these PFC liquids are given in Table I (Cuscó and Trusler, 1995; Hall *et al.*, 2000; Strohm and Kolios, 2011). Note that the surface tension listed is at the interface of the liquid and its vapor.

TABLE I. Physical properties of PFC liquids used in this study.

PFC name	Chemical Formula	Molecular weight (g/mol)	Bulk boiling point (°C)	Surface tension (mN/m)	Density (kg/m ³) 25 °C	Speed of sound (m/s) 25 °C	Compressibility (ms ² /Kg)
Perfluoropentane (PFP)	C ₅ F ₁₂	288.03	28–30	9.5	1590	477	2.77 × 10 ⁻⁹
Perfluorohexane (PFH)	C ₆ F ₁₄	338.04	58–60	12.23	1648	548	2.02 × 10 ⁻⁹
Perfluorooctyle bromide (PFOB)	C ₈ BrF ₁₇	498.96	142 °C	18	1930	630	1.3 × 10 ⁻⁹

The encapsulating shell contained lipids: 1,2-dipalmitoyl-sn-glycero-3-phosphatidylcholine (DPPC), 1,2-dipalmitoyl-sn-glycero-3-phosphate, sodium salt (DPPA), and 1,2-dipalmitoyl-sn-glycero-3-phosphoethanolamine-N-[methoxy-(polyethylene glycol)-5000] (MPEG5000 DPPE). All the lipids were purchased from Avanti Polar lipids (Alabaster, AL). A total lipid concentration of 2 mg/ml was maintained in the solution and the lipids were mixed in a molar ratio of 11:82:7 (DPPA: DPPC: MPEG5000DPPE) in a solution of phosphate buffered saline (PBS), propylene glycol and glycerol (8:1:1). These lipid components are similar to the ones used in Definity (Lantheus Medical Imaging, Inc., N. Billerica, MA, USA) microbubbles (Cheng, 2007). We followed an established lipid solution preparation protocol used by Hui *et al.* (2017). Briefly, to prepare the lipid solution, propylene glycol was heated to 10 °C above the gel-to-liquid transition temperature of the main phospholipid (DPPC) prior to contacting with the lipid blend. When the propylene glycol reached the desired temperature, lipids were added in the order of the least solubility—first DPPA, followed by DPPC, and then MPEG5000 DPPE. Lipid solution was heated and mechanically mixed for an hour (until the solution is clear). Meanwhile PBS and glycerol, heated to the same temperature separately, were added to the lipid blend dropwise. The mixture was later transferred into a preheated water bath (52 °C) for another hour of bath sonication (35 kHz, VWR, West Chester, PA). The lipid solution was stored at 4 °C and used within one week of preparation. Lipid-coated PFC droplets were prepared according to an established protocol (Kripfgans *et al.*, 2000). Briefly, 2 ml of the lipid solution was added into a 3-ml glass vial (Wheaton industries Inc., Millville, NJ). The vial was sealed with a rubber stopper (Wheaton Industries Inc.) and crimped. To remove the trapped air in the headspace and minimize generation of air bubbles, the vial was connected to a house vacuum pump for 30 s. Following that, 500 μl of PFC liquid was injected into the vial. Droplets of various PFC liquids were fabricated using a Vial Mixer (Bristol Myers Squibb, North Billerica, MA) shaken at 4800 rpm for 30 s. The vials were stored in the fridge and were used on the same day of preparation.

Since PFCs are denser than water (Table I), larger droplets would preferentially sediment to the bottom. To remove extremely large droplets (>30 μm in diameter), we diluted 2 ml of the droplet suspension (directly from the vial) with 13 ml degassed deionized (DI) water in a 15 ml centrifuge tube (column length of 12 cm) and kept it in the fridge in a vertical position for a predetermined time. The predetermined times were calculated according to Stokes equation: 5 min for PFP droplets, 4 min for PFH droplets, and 3 min for PFOB droplets, allowing droplets larger than 30 μm in

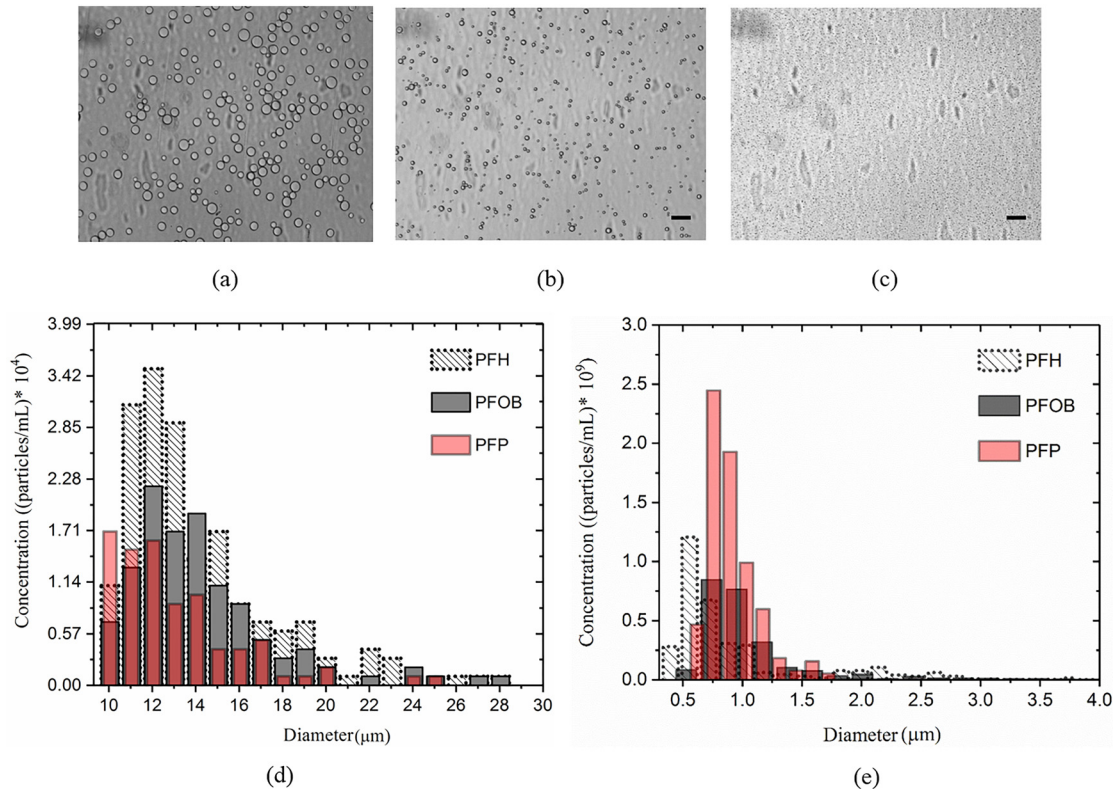


FIG. 1. (Color online) Light microscopic images of diluted (a) larger than $30\ \mu\text{m}$, (b) between 10 and $25\ \mu\text{m}$, (c) smaller than $4\ \mu\text{m}$ PFH droplets. Size distribution and concentrations of (d) large and (e) small groups of PFC droplets determined using qMicro and qNano systems. The scale bar is $50\ \mu\text{m}$.

diameter to settle (Feshitan *et al.*, 2009). Following that, the top $13\ \text{ml}$ of the diluted droplet suspension was transferred into a new $15\ \text{ml}$ centrifuge tube for the differential centrifugation process and the bottom $2\ \text{ml}$ containing extremely large droplets ($>30\ \mu\text{m}$) was discarded.

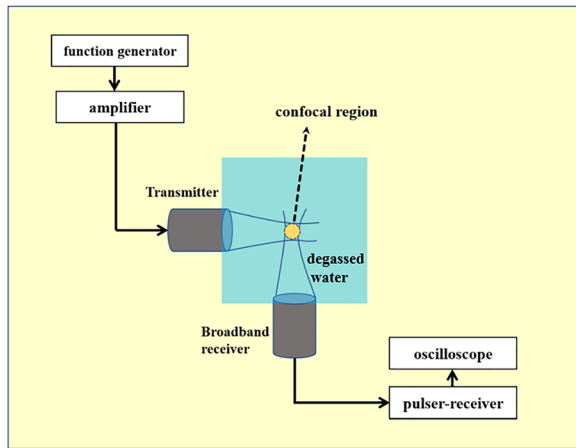
Droplets were then size isolated for diameters from 10 to $25\ \mu\text{m}$ (large droplet group) and smaller than $3\ \mu\text{m}$ (small droplet group) following a differential centrifugation technique detailed in the literature (Feshitan *et al.*, 2009; Mercado *et al.*, 2016). To collect droplets of size from 10 to $25\ \mu\text{m}$, the droplet suspension was centrifuged at $50\ \text{g}$ for $2\ \text{mins}$ for PFP and PFH droplets ($40\ \text{g}$ was used for PFOB since they are denser) using a bench type centrifuge (Eppendorf, NY). The top $3\ \text{ml}$ was discarded to get rid of potential bubbles formed during the mechanical agitation procedure. The bottom $2\ \text{ml}$ containing the target large droplets was transferred into a $50\ \text{ml}$ tube to be used for ADV experiments. To isolate droplets smaller than $3\ \mu\text{m}$, the middle $8\ \text{ml}$ of the suspension was transferred into a new tube for the second cycle of centrifugation at $60\ \text{g}$ for $1\ \text{min}$ for PFP, PFH, and PFOB droplets. Similarly, the top

$1\ \text{ml}$ was removed to get rid of potential bubbles and the middle $5\ \text{ml}$ was transferred into a $50\ \text{ml}$ tube to be used for the ADV experiments.

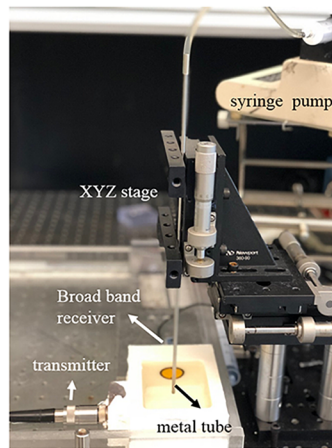
The size distribution and the concentration of small droplet group were determined using a qNano (Izon ScienceTM, Cambridge, MA). The droplet emulsion was diluted in PBS mixed with 0.03% Tween to ease passage of particles. For these measurements, we used three different elastomeric Poly-urethane nanopores (NP) that covered a size range of $200\text{--}1000\ \text{nm}$ (NP800), $1000\text{--}4000\ \text{nm}$ (NP2000), and $4000\text{--}10\ 000\ \text{nm}$ (NP4000). Before and after each measurement, NPs were calibrated using appropriate plain polystyrene particles (provided by Izon Company) of known size and number. In our case, the applied stretching values were kept between $45.5\text{--}47\ \text{mm}$. The voltage was set between 0.2 and $0.5\ \text{V}$ to keep the current approximately $125\ \text{nA}$. For each sample, 1000 particles were counted and analyzed using the qNano software. For the large droplet group, qMicro with micropore-membrane MP25 (size range of $5\text{--}25\ \mu\text{m}$) was used. For larger droplets, we also performed light microscopy image analysis

TABLE II. Average diameter of the droplets using qNano and qMicro measurements.

Liquid core	Small droplets		Large droplets	
	Diameter (nm)	Concentration (particles/ml)	Diameter (μm)	Concentration (particles/ml)
PFP	947 ± 45	6.1×10^9	11.99 ± 3.7	8.6×10^4
PFH	860 ± 100	3.4×10^9	14.21 ± 3.8	1.8×10^5
PFOB	954 ± 134	2.36×10^9	15.44 ± 3.4	1.18×10^5



(a)



(b)

FIG. 2. (Color online) (a) Schematic representation (horizontal plane showing the transducers confocally aligned is shown in top view). (b) Picture of the experimental setup used for determining ADV threshold. The droplet emulsion flows from an immersed metal tube [see (b)] 5 mm above the outer diameter of the transducers.

techniques which were in good agreement with qMicro results (data not shown). Figures 1(a)–1(c) show light microscope (AmScope FMA050, MA at 10 \times) images of isolated and diluted PFH droplets of size 30 μm , 10–25 μm , and smaller than 3 μm , respectively. Size measurement results with qMicro and qNano are shown in Figs. 1(d) and 1(e), respectively. Weighted average diameters of both small and large size droplets of different PFC liquids are summarized in Table II.

Droplet suspension was diluted 200 X and 50 X for small and large suspensions, respectively, prior to the ADV threshold determination experiments. The droplet suspension was then checked optically (microscope) and acoustically (see Sec. II B below) for any bubble presence.

B. Experimental setup for ADV and IC thresholds determination

For ADV experiments, typically the droplet suspension is passed through the focal volume of a transducer in a flow setup. In our previous work, we have shown that the focal volume is small ($\sim 4.21 \text{ mm}^3$ at 2.25 MHz) and it decreases with increasing frequency (Aliabouzar *et al.*, 2018). Similar to that work, here we have also used a tube-less setup to avoid wall effects (e.g., beam-diffraction, standing waves, reflection, and scattering from the wall) and any potential complex acoustic field at the focus. Figures 2(a) and 2(b) show a representation of our experimental setup for ADV threshold determination. A chamber (80 \times 60 \times 60 mm) made of polycarbonate was filled with degassed DI water. To perform ADV studies, we employed three spherically focused immersion transducers (Panametrics Transducer, Olympus NDT Corporation, Waltham, MA), each having an element diameter of 1.27 cm and a focal length of 3.05 cm as transmitters (f -number = 2.4). Transducers with central frequencies of 2.25 MHz (Model V306; -6 dB : 1.46–3.2 MHz), 10 MHz (Model V311; -6 dB : 6.96–13.16 MHz), and 15 MHz (Model V319; -6 dB : 10.10–18.97 MHz) were used as transmitters at their central frequencies. A broadband, cylindrically focused transducer (Sonic Concepts, Bothell, WA, USA) with an active diameter of 17.5 and 50 mm geometric focus was used as the receiver. This transducer had a flat frequency response between 10 kHz and 20 MHz. The transmitting and

receiving transducers were confocally positioned at right angles (Fig. 2). All the transducers were calibrated in a free field using a calibrated capsule hydrophone (HGL0200, dynamic range 1–20 MHz, Onda, Sunnyvale, CA).

For calibration, the transducer and the hydrophone were submerged in a water tank filled with degassed DI water. The pressure amplitudes at the focus of the transducers were measured and recorded with the capsule hydrophone at low driving voltages—from 0.15 to 0.6 MPa peak negative pressures. For higher peak negative pressures [from 0.6 to 4 MPa; Mechanical Index (MI) for the highest value is 2.6], to avoid hydrophone damage due to cavitation, nonlinear numerical modeling based on the Khokhlov-Zabolotskaya-Kuznetsov (KZK) equation was used. We have verified this calibration method by plotting the axial pressure distribution of a 2.25 MHz transducer (from the transducer surface up to a distance of 35 mm) at 450 kPa using the hydrophone and compared with the KZK simulations. The results were in good agreement (data not shown). This calibration technique has also been verified by Bessonova and Wilkens (2013) and Canney *et al.* (2008) using both fiber-optic hydrophone measurements and KZK predictions.

For ADV experiments, an arbitrary/function generator (Agilent, 33250A, Santa Clara, CA) was utilized to generate an 8-cycle sinusoidal pulse at a pulse repetition frequency (PRF) of 100 Hz. This signal was then amplified using a 55 dB power amplifier (A-150, ENI, Rochester, NY) and used to excite the transmitting transducer. The scattered signal was passively received by the receiving broadband transducer connected to a pulser/receiver (5800, Panametrics-NDT, Waltham, MA) in a receiving mode with a 20 dB gain (HP filter: 100 kHz, LP filter 35 MHz). The amplified signals were then fed into the oscilloscope (Tektronix, MDO3024, Beaverton, OR) to view them in real time. Signals were acquired directly from the oscilloscope using MATLAB (Mathworks, Natick, MA). Fifty voltage-time radio frequency (RF) traces were acquired in a sample mode and stored for further processing. Measurement for each setting was repeated five times.

To acoustically confirm that the freshly prepared droplet suspension was bubble-free, 20 μl of suspension was dispersed in the solution chamber and then was excited by ultrasound at an excitation pressure of 150 kPa, which was below

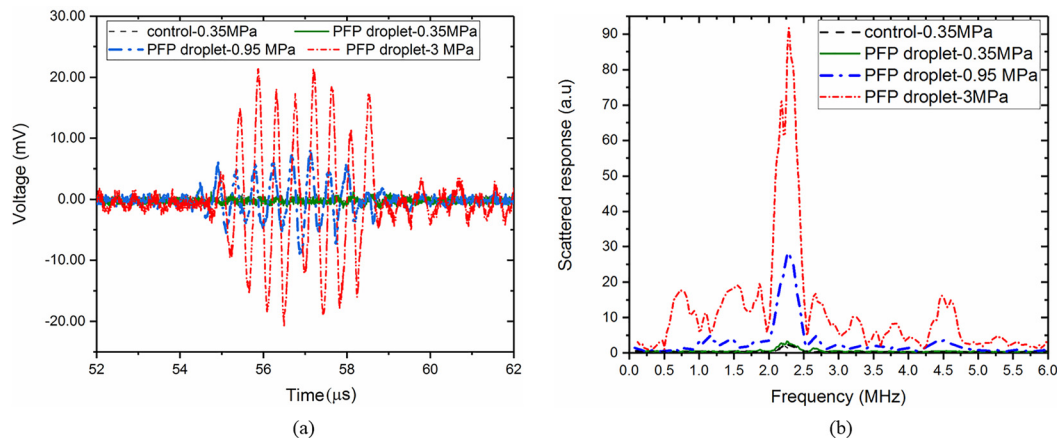


FIG. 3. (Color online) (a) RF trace of control and large PFP droplet signal at 0.35 MPa (below vaporization), 0.95 MPa (above vaporization without IC), and 3 MPa (above vaporization with IC); (b) corresponding fast Fourier transform from the control and the PFP droplet suspension at 2.25 MHz.

the minimum ADV thresholds found in this study. The scattered response was found to be comparable with that of the background noise confirming the suspension to be bubble free. Note that the current setup was found capable of detecting acoustical signals from even a very small amount (4μ l) of a microbubble suspension dispersed in the same chamber. A syringe pump (KD Scientific Inc, Holliston, MA) was used to inject the droplet suspension into the solution chamber with a flow rate and particle velocity of 20μ l/s and 2 mm/s, respectively. The syringe exit was connected to a stainless steel tube (inner diameter 2.9 mm). The tube exit was immersed in the solution chamber and mounted approximately 5 mm above the outer diameter of the transducers. The distance was sufficient so that the steel tube would not generate any signal. The steel tube was attached to the manual linear translation stage (Newport Corporation, Irvine, CA) having a precision of 1μ m in all three directions. The dimensions of the focal region for a given frequency has been calculated by the formulae from the transducer manual (Olympus, 2006). We ensured that the stream of droplets passed through the intersecting focal volume by first injecting a stream of propylene glycol (higher acoustic impedance of 1.61 MRayl compared to that of water 1.48 MRayl) into the solution chamber via the steel tube to determine the proper position of the tube. When the steel tube was properly mounted so that the stream of propylene glycol passed through the focal volume, we obtained a strong signal. The positioning procedure was repeated before each experiment. All experiments were performed at 37°C . PFOB droplets, due to higher bulk boiling point of 142°C , did not experience ADV at 37°C ; the experiments for PFOB droplets were repeated at 43°C . Degassed DI water and the droplet suspensions were kept in water bath heated to the desired temperature and allowed to reach equilibrium. To determine the ADV threshold, the excitation pressure was increased in steps of 200 kPa for each excitation frequency from 100 kPa to 4 MPa.

C. Criterion for deciding the acoustic droplet vaporization and inertial cavitation thresholds

Liquid droplets are poor scatterers of ultrasound while microbubbles are far stronger scatterers. The scattering

cross-section of a bubble is several orders of magnitude higher than that of a liquid droplet of the same size (Medwin and Clay, 1997). The acoustic behavior of gas bubbles is mainly dominated by the resonance. Around the resonant frequency the effects of backscattering and absorption are much enhanced (Sarkar and Prosperetti, 1994). Furthermore, upon vaporization, the droplet undergoes volumetric expansion of about 125 fold, as shown by Rapoport *et al.* (2009) and Sheeran *et al.* (2011), resulting in a sudden jump in their scattered response. Here, we plotted peak-to-peak, fundamental, and non-linear components, such as sub or second harmonics (when present) as the ultrasound excitation amplitude was progressively increased.

For IC studies, experiments were done in the same setup. Inertial cavitation is accompanied by a broadband noise. The IC threshold here was defined as the amplitude at which the integrated power calculated in the low frequency range, from 500 to 900 kHz, increased from the baseline. Note that the low frequency emission has been used as IC criterion in several past studies (Giesecke and Hynynen, 2003; Fabiilli *et al.*, 2009; Moncion *et al.*, 2016). Figure 3 represents raw RF data along with the corresponding frequency spectrum for the control (base lipid solution) and the droplet signals at three different excitation amplitudes of 0.35 MPa (below ADV), 0.95 MPa (above ADV/without IC), and 3 MPa (above ADV with IC) at 2.25 MHz for large PFP droplets. The droplet signal at 0.35 MPa was very close to the control. For an excitation pressure 0.95 MPa, above the ADV threshold, the droplet signal became substantially higher than the control. This sharp increase can also be noted in the corresponding frequency spectrum. We found that the peak-to-peak voltage, fundamental and nonlinear components (if present) all increased from the baseline readings and continued to be high for all the subsequent amplitudes. For an objective definition of the threshold values, data were segmented between, before, and after a sudden increase and then a piece-wise linear fit was performed on each segment using OriginLab (OriginPro8, OriginLab, Northampton, MA). The ADV as well as IC thresholds were defined as the peak negative pressure corresponding to the intersection of the first two segmental lines of the piece-wise linear fit. Such

methods of threshold determination have been used in several past studies (Radhakrishnan *et al.*, 2013; Radhakrishnan *et al.*, 2016; Moncion *et al.*, 2017). In view of the stochastic nature, the ADV threshold values, although determined here as in the previous investigations through a quantitative method, are to be understood as a representative of the values of excitation where vaporization occurs, rather than a precise single value, with no vaporization below that range.

D. Statistical analysis

All the scattered responses were presented as the mean of the data sets acquired at each setting and their corresponding standard deviations. All experiments at each driving pressure and frequency were repeated five times. A Kolmogorov-Smirnov test was performed on the data to ensure a normal distribution. Finally, the ADV threshold values from different criteria (scattered responses) were averaged.

III. RESULTS AND DISCUSSION

A. Acoustic droplet vaporization at 2.25 MHz

Figures 4(a), 4(b), 4(c), and 4(d) plot the peak-to-peak voltage, fundamental, sub, and second harmonic responses, respectively, from the droplet suspensions of PFP, PFH, and PFOB from the large size distribution group at the excitation frequency of 2.25 MHz.

The signal from the droplet suspension was comparable to the control signal at excitation amplitudes below 0.4 MPa for PFP droplets and 2.3 MPa for PFH droplets in the plots. In Fig. 4(a), the intersection of the first two segments of the piece-wise linear fit (ADV threshold) happens at 0.4 MPa ($R^2 = 0.99$) and 2.3 MPa ($R^2 = 0.98$) for PFP and PFH droplets, respectively. This was using the peak-to-peak data. The fundamental component shown in Fig. 4(b) resulted in very similar values of the threshold—0.39 MPa ($R^2 = 0.99$) and 2.27 MPa ($R^2 = 0.98$) for PFP and PFH droplets, respectively. Note that the experiments were performed at 37 °C. We did not observe any vaporization for PFOB droplets at 37 °C (data not shown) for the excitation pressures (up to 4 MPa) studied here. Even at 43 °C, PFOB droplets failed to vaporize [response is same as control in Figs. 4(a) and 4(b)]. Note that the scattered fundamental response from PFP droplets post ADV seemed to saturate at higher amplitude, a phenomenon also seen previously in ADV studies of PFP droplets (Reznik *et al.*, 2011). Similar saturation was also observed in experimental measurement as well as numerical prediction of scattered responses from coated microbubbles (Sarkar *et al.*, 2005; Paul *et al.*, 2010; Paul *et al.*, 2013; Paul *et al.*, 2014).

Using a similar procedure on the sub- and second-harmonic components [Figs. 4(c) and 4(d)] for the large droplet suspension, we obtained the same threshold values of 0.41 [$R^2 = 0.93$] and 0.36 ($R^2 = 0.98$) for PFP droplets as in

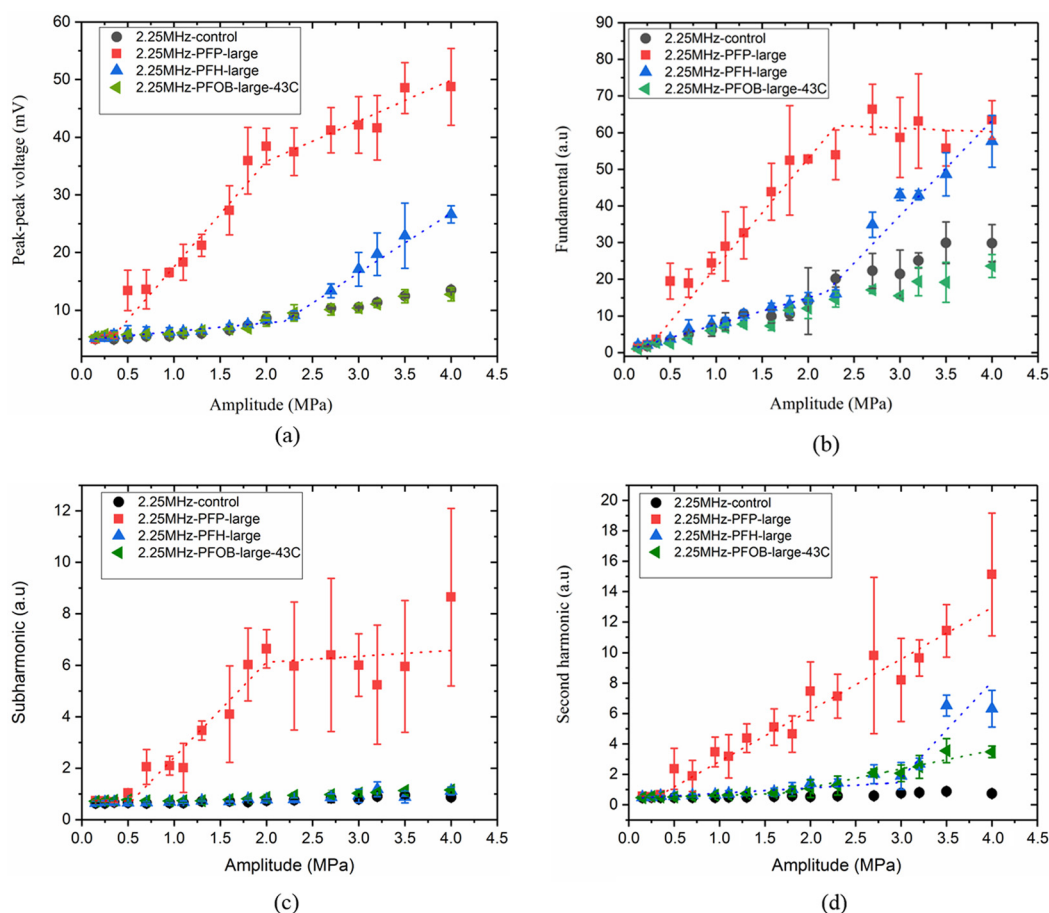


FIG. 4. (Color online) (a) Peak-to-peak voltage, (b) fundamental, (c) subharmonic, and (d) second harmonic components of the scattered response for large droplets with PFP, PFH, and PFOB (at 43 °C) liquid cores at the excitation frequency of 2.25 MHz.

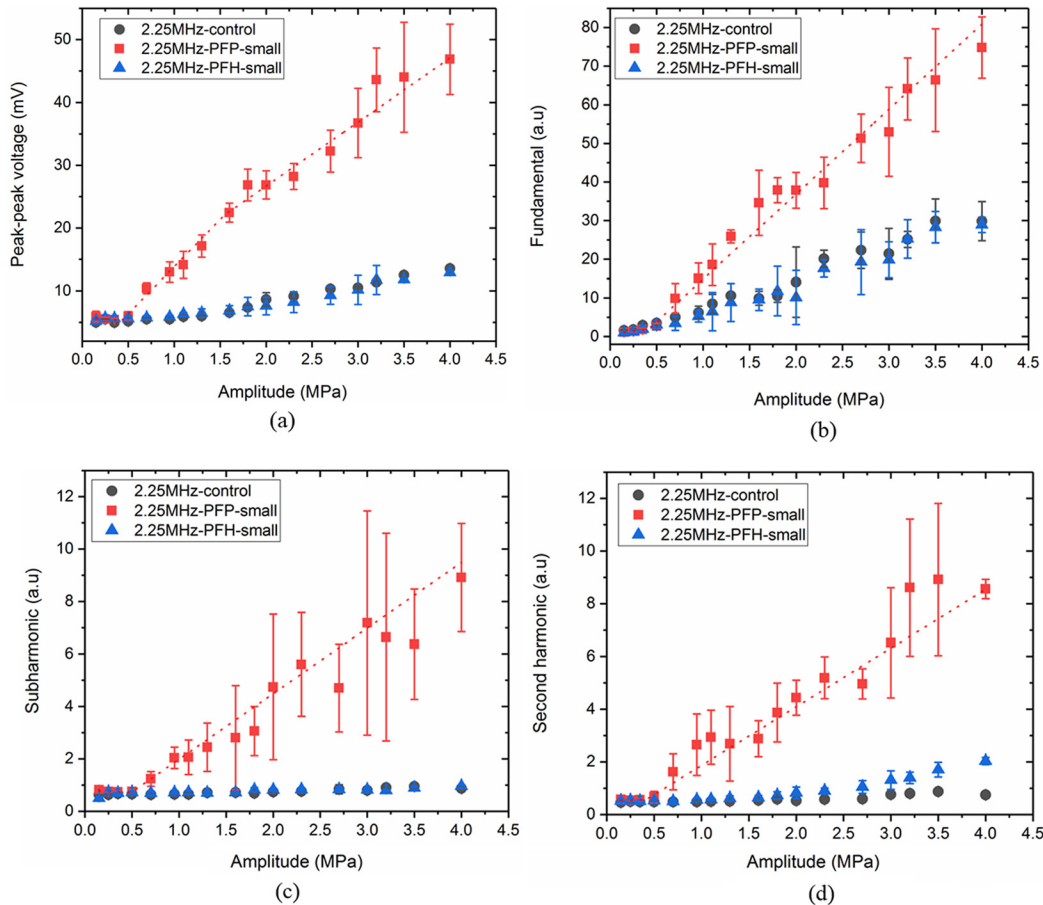


FIG. 5. (Color online) (a) Peak-to-peak, (b) fundamental, (c) sub, and (d) second harmonic components for suspensions of small droplets with various PFC cores at 2.25 MHz.

Figs. 4(a) and 4(b)]. However, PFH droplets did not generate any subharmonic response. Note that PFH droplets, with boiling point higher than the operating temperature, have been observed by optical means to undergo repeated vaporization and re-condensation in response to irradiation by near-infrared laser pulses (Hannah *et al.*, 2016). B-mode observations of similar phenomenon (Asami and Kawabata, 2012) also reported a transient vaporization of PFH droplets compared to PFP droplets. The transient nature of the vaporization or re-condensation and therefore not enough time for sustained oscillation could be the reason for the lack of subharmonic response. PFH is a stronger liquid (i.e., one with higher boiling point and surface tension, see Table I) compared to PFP, and therefore requires substantially higher amplitude (2.3 MPa peak negative pressure compared to 0.4 MPa peak negative pressure for PFP at this frequency) for vaporization. At 2.3 MPa peak rarefactional pressure, the peak compressional pressure is also much higher (4.25 MPa), which might be another reason to favor re-condensation of PFH droplets. Note that, at the ambient temperature of 37 °C, PFP is superheated according to their bulk boiling point while PFH is not. Incidentally, repeated vaporization and re-condensation offer potential applications where extended imaging or drug delivery is required (Asami and Kawabata, 2012). Figure 4(d) displays the second harmonic generation at 2.25 MHz. Similar to other scattered responses, second harmonic also rose at 0.36 MPa for PFP. For PFH droplets, this jump was noticeable

above 2.9 MPa. However, at this high excitation, second harmonic response can also be due to nonlinear propagation of ultrasound in water (Clay and Medwin, 1977) rather than from bubble activities. Specifically, for PFOB droplets at 43 °C, we see an increase in second harmonic response, although, as already noted above, these droplets did not register any increase in other scattered components. In our previous study, we investigated the contribution of nonlinear propagation in water by recording the second harmonic response from a non-vaporizing liquid propylene glycol stream. The effect of nonlinear propagation was not pronounced for lower amplitudes (below 2.5 MPa) but it slowly built up at higher amplitudes at this excitation frequency (Aliabouzar *et al.*, 2018).

In our previous study (Aliabouzar *et al.*, 2018), analyzing scattered responses at different frequency components—fundamental, sub-, and second-harmonic—resulted in similar but slightly different ADV thresholds. There, we measured different scattered components performing separate experiments using different narrowband transducers as receiver. In contrast, here we used a broadband transducer and the different frequency components gave rise to virtually same ADV threshold values for both sizes and all excitation frequencies (see also below).

In Fig. 5, we plot peak-to-peak, fundamental, sub-, and second-harmonic responses for the small droplets of PFP and PFH droplets at 2.25 MHz. Similar to the large droplets the procedure applied to the peak-to-peak,

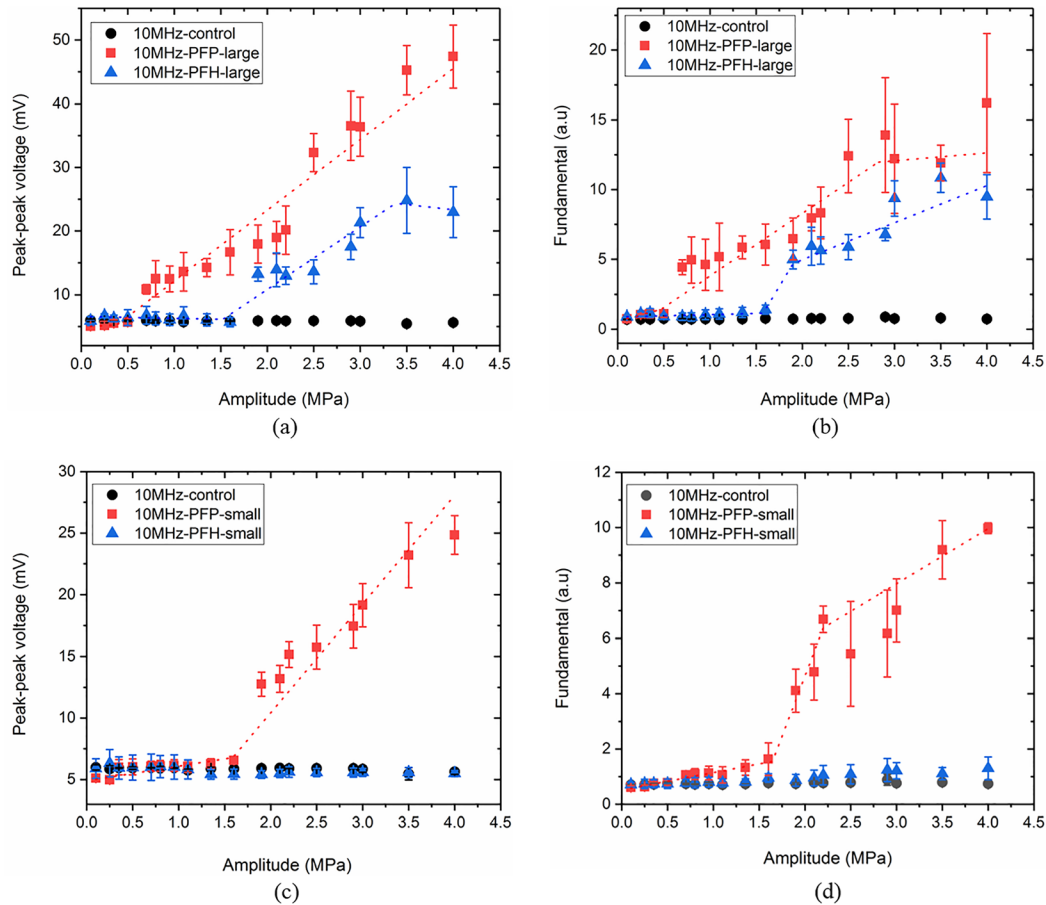


FIG. 6. (Color online) (a) Peak-to-peak and (b) fundamental responses of suspensions of large droplets, (c) peak-to-peak and (d) fundamental responses from small droplets at the excitation frequency of 10 MHz.

fundamental, sub-, and second-harmonic data resulted in very similar values of threshold for PFP small droplets: 0.52 MPa ($R^2=0.97$), 0.56 MPa ($R^2=0.99$), 0.5 MPa ($R^2=0.99$), and 0.49 MPa ($R^2=0.99$), respectively. No vaporization was observed for small PFH and PFOB (data not shown) droplets (up to 4 MPa). For PFOB, we also repeated the experiments at 43 °C and did not record any vaporization (data not shown).

Comparing Figs. 4 and 5, one can notice the effect of droplet size on average ADV threshold for each droplet suspension at 2.25 MHz. The ADV threshold increased from 0.39 MPa for large PFP to 0.52 MPa for small PFP droplets. For PFH, while large droplets recorded 2.28 MPa, no vaporization was observed for small droplets.

The threshold of vaporization for small PFP droplets at 37 °C (0.52 MPa) was lower compared to the one we reported in the previous study at room temperature (1.05 MPa) as can be expected (Zhang and Porter, 2010; Reznik *et al.*, 2011). Higher boiling point PFC liquids such as PFH and PFOB have not been explored as much due to the low efficiency of vaporization. Zhang and Porter (2010) observed no vaporization for H-PFP (2H, 3H-perfluoropentane; boiling point of 56 °C) droplets having an average diameter of $690 \pm 233 \mu\text{m}$ at the excitation frequency of 2 MHz up to pressure values as high as 8 MPa. Moncion *et al.* (2017) reported a threshold value of 2.2 MPa for double emulsions of size $13.9 \pm 0.04 \mu\text{m}$ made of PFH liquid at 2.5 MHz.

B. Acoustic droplet vaporization at 10 MHz

Figures 6(a) and 6(b) plot the peak-to-peak voltage and the fundamental response from large PFP and PFH droplet groups as functions of peak negative pressure at 10 MHz excitation frequency. At this frequency, thresholds of vaporization were 0.58 ($R^2=0.99$) [Fig. 6(a)] and 0.56 ($R^2=0.92$) [Fig. 6(b)] for large PFP and 1.52 ($R^2=0.91$) [Fig. 6(a)] and 1.58 MPa ($R^2=0.97$) [Fig. 6(b)] for large PFH droplets. For small PFP droplets, ADV threshold was recorded as 1.58 MPa ($R^2=0.93$) and 1.66 MPa ($R^2=0.99$) in Figs. 6(c) and 6(d), respectively. We did not detect any vaporization for small PFH droplet group at this excitation frequency (up to 4 MPa) similar to 2.25 MHz. Similarly, no vaporization of either small or large PFOB droplets (even at 43 °C) was detected at this frequency either (data not shown). At the excitation frequency of 10 MHz, we did not detect subharmonic response from the droplet suspensions at the vaporization threshold, as was also the case in our previous paper, possibly due to the fact that subharmonic response from a bubble is frequency and threshold dependent (Katiyar and Sarkar, 2011).

C. Acoustic droplet vaporization at 15 MHz

At the excitation frequency of 15 MHz, Fig. 7(a) recorded ADV vaporization thresholds of 1.09 MPa ($R^2=0.99$), 1.12 MPa ($R^2=0.98$) and 2.8 MPa ($R^2=0.87$) for large PFP,

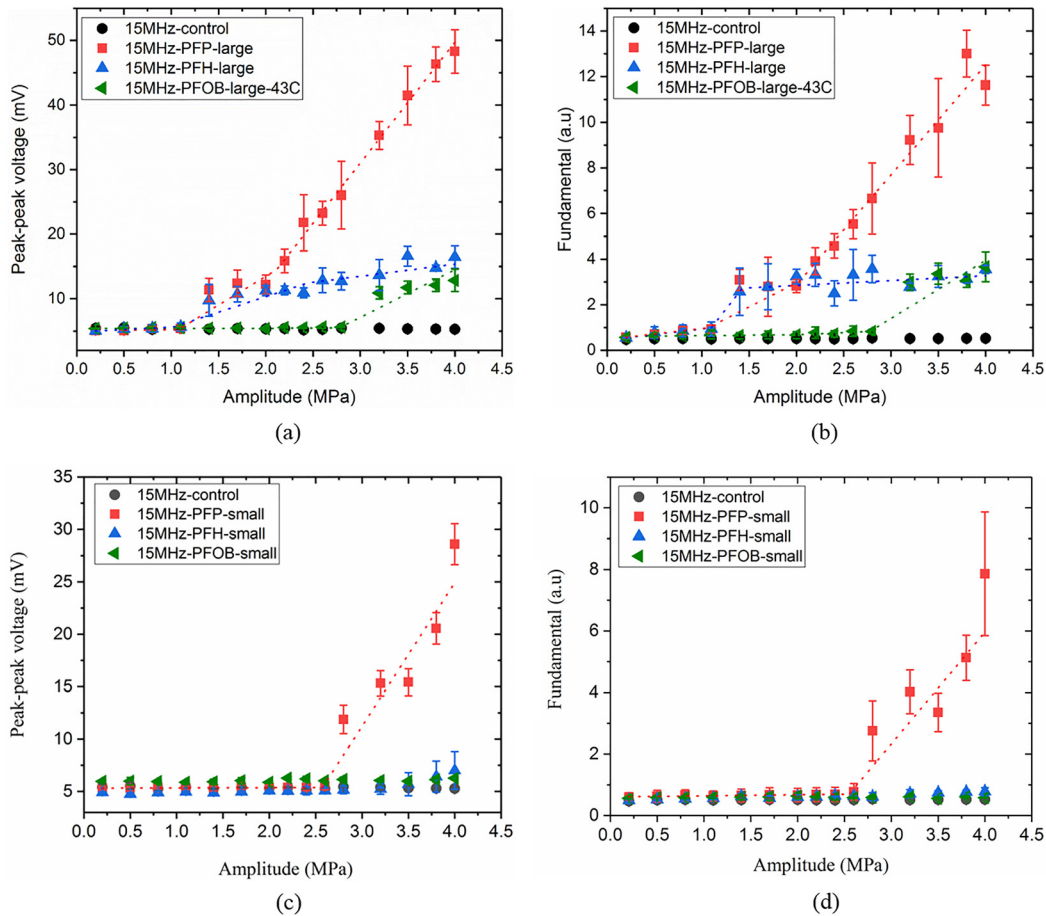


FIG. 7. (Color online) (a) Peak-to-peak, (b) fundamental response from large PFC droplets, (c) peak-to-peak, and (d) fundamental response from small PFC droplets at the excitation frequency of 15 MHz.

PFH, and PFOB (only at 43 °C) droplets using the peak-to-peak response. Corresponding values from fundamental response were again very similar—1.06 MPa ($R^2=0.97$), 1.1 MPa ($R^2=0.98$) and 2.77 MPa ($R^2=0.91$), respectively [Fig. 7(b)]. The small droplets expectedly showed a higher value of ADV threshold—2.57 MPa ($R^2=0.96$) for PFP droplet [Fig. 7(c)]. This one was from the peak-to-peak response, which was again very similar to the one obtained from fundamental is 2.55 MPa ($R^2=0.93$) [Fig. 7(d)]. No vaporization was detected for small PFH and PFOB droplets.

Matsuura *et al.* (2009) reported an ADV threshold of 4.7 MPa for PFH droplets at the excitation frequency of 18 MHz in a cellulose tube positioned at the focus of the linear array. Note that direct comparison cannot be made due to the differences in droplet sizes, and experimental setup. However, the higher value in their study might partially be due to increased attenuation across the wall of the cellulose tube.

D. Frequency dependence of ADV threshold on size and boiling point of PFCs

As noted in the Introduction, previous studies of the frequency dependence of ADV thresholds of PFC liquid droplets have been contradictory. Here, we have combined the effects of size and liquid core properties on the dependence

of ADV threshold on the frequency of excitation. We have recorded an increasing trend of vaporization threshold with frequency for both small and large PFP (the most volatile liquid considered here with the bulk boiling point of 29 °C and surface tension of 9.5 mN/m) droplets. The increasing trend of the ADV threshold with increasing frequency can be reasoned as arising from longer duration of continuous negative pressure that the droplets experience at lower frequency, which in turn would increase the probability of nucleation. According to homogenous nucleation theory, liquid under negative pressure is metastable and given sufficient time vapor bubbles nucleate and expand (Church, 2002). As noted before, ADV increasing with frequency of excitation has been reported in our previous paper for PFP droplets at 20 °C as well as by others (Kripfgans *et al.*, 2004; Martin *et al.*, 2012; Sheeran *et al.*, 2013).

However, here we also observed an opposite trend for a higher boiling point PFC liquid, PFH—ADV threshold decreases with frequency of excitation for large droplet group as shown in Fig. 8. PFOB large droplets did not vaporize at lower frequencies in the range of excitations (<4 MPa) considered here, but registered a threshold of 2.8 MPa at 15 MHz (also at 43 °C). Note that PFH and PFOB are stronger liquids, i.e., with higher boiling points and surface tensions than PFP. They require much higher peak rarefactional pressures for vaporization where we expect to have

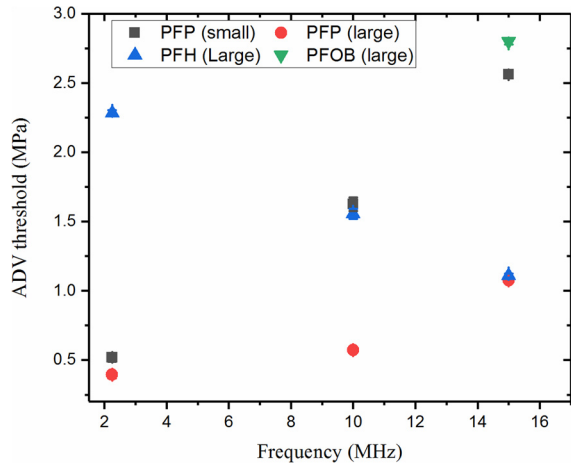


FIG. 8. (Color online) ADV thresholds of PFC droplets as a function of frequency of excitation for PFP small and large (37 °C), PFH large (37 °C), and PFOB large (43 °C) groups.

significant amount of nonlinearity. Therefore, superharmonic focusing possibly took place at these high amplitudes for large PFH and PHOB droplets. Superharmonic focusing has been optically shown to be pronounced for larger droplets (radius $>4 \mu\text{m}$), higher frequencies and higher amplitudes (Shpak *et al.*, 2014). It is noteworthy that we see both trends—ADV threshold increasing and decreasing with

excitation frequency depending on size and droplet core. It shows that both size and material properties of the liquid core, such as boiling point and surface tension, play a critical role in defining the trend of vaporization with frequency of excitation. The average thresholds for the emulsions of different sizes and liquid cores are summarized in Fig. 8. Note that the MI calculated for this system ranged from 0.26 (0.39 MPa at 2.25 MHz for large PFP droplets) to 1.51 (2.27 MPa at 2.25 MHz for large PFH droplets).

E. Inertial cavitation

For the IC threshold measurements, we plot the integrated power spectrum within 500–900 kHz frequency interval (Fig. 9). Similar to ADV threshold detection, piece-wise linear fitting was performed on the data points to find the IC threshold. We have plotted the integrated power-frequency spectrum for both small and large groups of PFP droplets at 2.25 MHz [Fig. 9(a)], 10 MHz [Fig. 9(b)], and 15 MHz [Fig. 9(c)]. IC thresholds are as follows: at 2.25 MHz, 1.6 MPa ($R^2=0.96$) for small PFP and 1.12 MPa ($R^2=0.91$) for large PFP droplets; at 10 MHz, 2.77 MPa ($R^2=0.86$) for small PFP and 2.09 MPa ($R^2=0.84$) for large PFP droplets; at 15 MHz: 3.47 MPa ($R^2=0.7$) for small PFP and 2.57 MPa ($R^2=0.86$) for large PFP droplets. At each frequency, as expected, IC threshold for larger droplets are higher than

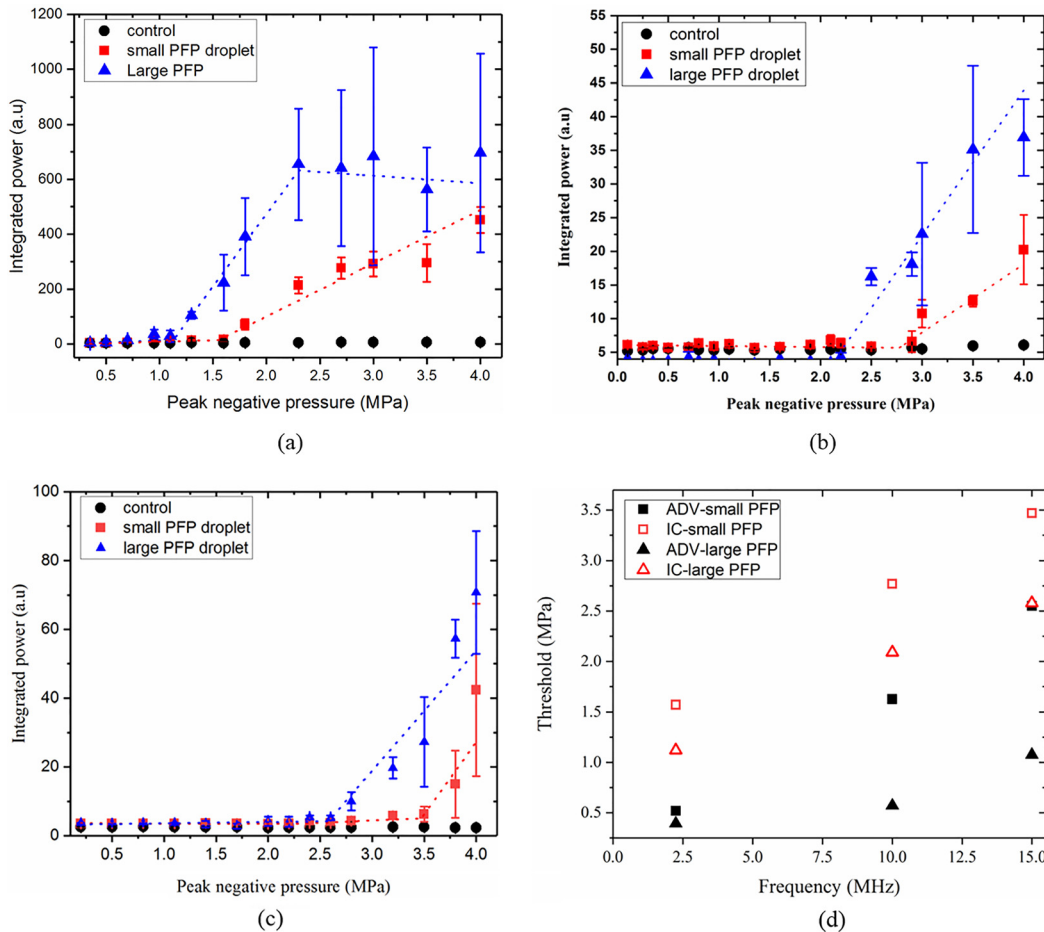


FIG. 9. (Color online) IC threshold at (a) 2.25 MHz, (b) 10 MHz and (c) 15 MHz for small as well as large PFP droplets, and (d) comparison of IC and ADV for small and large PFP droplets at various frequencies.

that of the smaller droplets, and IC threshold is always higher than that for ADV [Fig. 9(d)]. For PFH and PFOB cases, no IC was recorded for the pressures studied here. Moncion *et al.* (2017) reported an IC threshold value of 4.8 MPa for double emulsions of PFH droplets of similar size (14 μm) at 2.5 MHz within a fibrin gel. An IC threshold of 1.5 MPa was reported for both PFP and PFH droplets of 2 μm in diameter by Giesecke and Hynynen (2003) at 2.18 MHz.

IV. CONCLUSION

We systematically studied the effect of frequency of excitation on the threshold of vaporization by performing ADV experiments on lipid coated droplets of different sizes and liquid cores. Progressively increasing the peak negative excitation amplitude, we found a simultaneous sharp change in peak-to-peak, fundamental, sub- and second harmonic scattered responses at a certain value of the excitation, indicating vaporization. The ADV threshold, where the sharp change in the scattered responses occurs, was found to increase with frequency for both small and large size PFP droplets (the most volatile PFC liquid studied here). For large PFH droplets—small ones did not vaporize in the excitation range (up to 4 MPa) considered—the ADV threshold decreased with frequency. The large PFOB droplets vaporized only at the highest frequency (15 MHz), indicating the same trend. Note that, while the increasing trend of ADV threshold with frequency is due to increased probability of nucleation, the decreasing trend for larger droplets and higher boiling point liquids may be due to superharmonic focusing facilitated by the nonlinearity at the higher excitation in those cases as well as larger droplet radii. These findings show that both size and physical properties of the liquid core such as boiling point and surface tension play a critical role in defining the trend of vaporization with frequency of excitation. IC was measured by calculating the integrated power frequency spectrum in the range from 500 to 900 kHz. IC was observed only for PFP droplets (under peak negative pressures up to 4 MPa) and it increased with the frequency of excitation and was lower for larger droplet sizes. For all the frequencies studied here, ADV thresholds were lower than the IC thresholds.

ACKNOWLEDGMENTS

We would like to thank Dr. A. Pal and A. Senthikumar from Izon Science Ltd for performing the qMicro size measurements. K.S. acknowledges partial support from NSF Grant Nos. CBET-1205322, CBET 1603639, and NIH R01GM114080, and George Washington University CDRF.

Aliabouzar, M., Kumar, K. N., and Sarkar, K. (2018). "Acoustic vaporization threshold of lipid-coated perfluoropentane droplets," *J. Acoust. Soc. Am.* **143**, 2001–2012.

Apfel, R. E., and Holland, C. K. (1991). "Gauging the likelihood of cavitation from short-pulse, low-duty cycle diagnostic ultrasound," *Ultrasound Med. Biol.* **17**, 179–185.

Asami, R., and Kawabata, K. (2012). "Repeatable vaporization of optically vaporizable perfluorocarbon droplets for photoacoustic contrast enhanced imaging," in *Proceedings of the 2012 IEEE International Ultrasonics Symposium (IUS)*, October 7–10, Dresden, Germany, pp. 1200–1203.

Bessonova, O. V., and Wilkens, V. (2013). "Membrane hydrophone measurement and numerical simulation of HIFU fields up to developed shock regimes," *IEEE Trans. Ultrason. Ferroelectr. Freq. Control* **60**, 290–300.

Canney, M. S., Bailey, M. R., Crum, L. A., Khokhlova, V. A., and Sapozhnikov, O. A. (2008). "Acoustic characterization of high intensity focused ultrasound fields: A combined measurement and modeling approach," *J. Acoust. Soc. Am.* **124**, 2406–2420.

Cheng, K. T. (2007). "Perflutren lipid microspheres," Molecular Imaging and Contrast Agent Database (MICAD), Bethesda, MD.

Church, C. C. (2002). "Spontaneous homogeneous nucleation, inertial cavitation and the safety of diagnostic ultrasound," *Ultrasound Med. Biol.* **28**, 1349–1364.

Clay, C. S., and Medwin, H. (1977). *Acoustical Oceanography: Principles and Applications* (Wiley, New York).

Cuscó, L., and Trusler, J. (1995). "Identification of environmentally acceptable low-sound speed liquids," *Int. J. Thermophys.* **16**, 675–685.

Fabiilli, M. L., Haworth, K. J., Fakhri, N. H., Kripfgans, O. D., Carson, P. L., and Fowlkes, J. B. (2009). "The role of inertial cavitation in acoustic droplet vaporization," *IEEE Trans. Ultrason. Ferroelectr. Freq. Control* **56**, 1006–1017.

Fabiilli, M. L., Haworth, K. J., Sebastian, I. E., Kripfgans, O. D., Carson, P. L., and Fowlkes, J. B. (2010). "Delivery of chlorambucil using an acoustically-triggered perfluoropentane emulsion," *Ultrasound Med. Biol.* **36**, 1364–1375.

Ferrara, K., Pollard, R., and Borden, M. (2007). "Ultrasound microbubble contrast agents: Fundamentals and application to gene and drug delivery," *Ann. Rev. Biomed. Eng.* **9**, 415–447.

Feshitan, J. A., Chen, C. C., Kwan, J. J., and Borden, M. A. (2009). "Microbubble size isolation by differential centrifugation," *J. Colloid Interf. Sci.* **329**, 316–324.

Giesecke, T., and Hynynen, K. (2003). "Ultrasound-mediated cavitation thresholds of liquid perfluorocarbon droplets in vitro," *Ultrasound Med. Biol.* **29**, 1359–1365.

Hall, C. S., Lanza, G. M., Rose, J. H., Kaufmann, R. J., Fuhrhop, R. W., Handley, S. H., Waters, K. R., Miller, J. G., and Wickline, S. A. (2000). "Experimental determination of phase velocity of perfluorocarbons: Applications to targeted contrast agents," *IEEE Trans. Ultrason. Ferroelectr. Freq. Control* **47**, 75–84.

Hannah, A. S., Luke, G. P., and Emelianov, S. Y. (2016). "Blinking phase-change nanocapsules enable background-free ultrasound imaging," *Theranostics* **6**, 1866–1876.

Hui, P. K., Bishop, J. E., and Madrigal, E. S., Jr., (2017). "Preparation of a lipid blend and a phospholipid suspension containing the lipid blend," U.S. patent no. 20010003580A1.

Katiyar, A., and Sarkar, K. (2011). "Excitation threshold for subharmonic generation from contrast microbubbles," *J. Acoust. Soc. Am.* **130**, 3137–3147.

Katiyar, A., Sarkar, K., and Jain, P. (2009). "Effects of encapsulation elasticity on the stability of an encapsulated microbubble," *J. Colloid Interf. Sci.* **336**, 519–525.

Kopechek, J. A., Park, E., Mei, C.-S., McDannold, N. J., and Porter, T. M. (2013). "Accumulation of phase-shift nanoemulsions to enhance MR-guided ultrasound-mediated tumor ablation in vivo," *J. Healthcare Eng.* **4**, 109–126.

Kripfgans, O. D., Carson, P. L., and Fowlkes, J. B. (2002). "On the mechanism of acoustic droplet vaporization," in *Proceedings of the 2002 IEEE Ultrasonics Symposium*, October 8–11, Munich, Germany, pp. 535–538.

Kripfgans, O. D., Fabiilli, M. L., Carson, P. L., and Fowlkes, J. B. (2004). "On the acoustic vaporization of micrometer-sized droplets," *J. Acoust. Soc. Am.* **116**, 272–281.

Kripfgans, O. D., Fowlkes, J. B., Miller, D. L., Eldevik, O. P., and Carson, P. L. (2000). "Acoustic droplet vaporization for therapeutic and diagnostic applications," *Ultrasound Med. Biol.* **26**, 1177–1189.

Li, D. S., Kripfgans, O. D., Fabiilli, M. L., Brian Fowlkes, J., and Bull, J. L. (2014). "Initial nucleation site formation due to acoustic droplet vaporization," *Appl. Phys. Lett.* **104**, 063703.

Lo, A. H., Kripfgans, O. D., Carson, P. L., Rothman, E. D., and Fowlkes, J. B. (2007). "Acoustic droplet vaporization threshold: Effects of pulse duration and contrast agent," *IEEE Trans. Ultrason. Ferroelectr. Freq. Control* **54**, 933–946.

Martin, A. L., Seo, M., Williams, R., Belayneh, G., Foster, F. S., and Matsuura, N. (2012). "Intracellular growth of nanoscale perfluorocarbon droplets for enhanced ultrasound-induced phase-change conversion," *Ultrasound Med. Biol.* **38**, 1799–1810.

- Matsuura, N., Williams, R., Gorelikov, I., Chaudhuri, J., Rowlands, J., Hynynen, K., Foster, S., Burns, P., and Resnik, N. (2009). "Nanoparticle-loaded perfluorocarbon droplets for imaging and therapy," in *Proceedings of the 2009 IEEE International Ultrasonics Symposium (IUS)*, September 20–23, Roma, Italy, pp. 5–8.
- Medwin, H., and Clay, C. S. (1997). *Fundamentals of Acoustical Oceanography* (Academic Press, New York).
- Mercado, K. P., Radhakrishnan, K., Stewart, K., Snider, L., Ryan, D., and Haworth, K. J. (2016). "Size-isolation of ultrasound-mediated phase change perfluorocarbon droplets using differential centrifugation," *J. Acoust. Soc. Am.* **139**, EL142–EL148.
- Miles, C. J., Doering, C. R., and Kripfgans, O. D. (2016). "Nucleation pressure threshold in acoustic droplet vaporization," *J. Appl. Phys.* **120**, 034903.
- Moncion, A., Arlotta, K. J., Kripfgans, O. D., Fowlkes, J. B., Carson, P. L., Putnam, A. J., Franceschi, R. T., and Fabiilli, M. L. (2016). "Design and characterization of fibrin-based acoustically responsive scaffolds for tissue engineering applications," *Ultrasound Med. Biol.* **42**, 257–271.
- Moncion, A., Lin, M., O'Neill, E. G., Franceschi, R. T., Kripfgans, O. D., Putnam, A. J., and Fabiilli, M. L. (2017). "Controlled release of basic fibroblast growth factor for angiogenesis using acoustically-responsive scaffolds," *Biomaterials* **140**, 26–36.
- Olympus, N. (2006). "Ultrasonic transducers technical notes," Technical Brochure: Olympus NDT, Waltham, MA, 2.2.
- Paul, S., Katiyar, A., Sarkar, K., Chatterjee, D., Shi, W. T., and Forsberg, F. (2010). "Material characterization of the encapsulation of an ultrasound contrast microbubble and its subharmonic response: Strain-softening interfacial elasticity model," *J. Acoust. Soc. Am.* **127**, 3846–3857.
- Paul, S., Nahire, R., Mallik, S., and Sarkar, K. (2014). "Encapsulated microbubbles and echogenic liposomes for contrast ultrasound imaging and targeted drug delivery," *Comput. Mech.* **53**, 413–435.
- Paul, S., Russakow, D., Rodgers, T., Sarkar, K., Cochran, M., and Wheatley, M. A. (2013). "Determination of the interfacial rheological properties of a Poly(DL-lactic acid)-encapsulated contrast agent using in vitro attenuation and scattering," *Ultrasound Med. Biol.* **39**, 1277–1291.
- Radhakrishnan, K., Bader, K. B., Haworth, K. J., Kopechek, J. A., Raymond, J. L., Huang, S.-L., McPherson, D. D., and Holland, C. K. (2013). "Relationship between cavitation and loss of echogenicity from ultrasound contrast agents," *Phys. Med. Biol.* **58**, 6541–6563.
- Radhakrishnan, K., Holland, C. K., and Haworth, K. J. (2016). "Scavenging dissolved oxygen via acoustic droplet vaporization," *Ultrason. Sonochem.* **31**, 394–403.
- Rapoport, N. Y., Efros, A. L., Christensen, D. A., Kennedy, A. M., and Nam, K.-H. (2009). "Microbubble generation in phase-shift nanoemulsions used as anticancer drug carriers," *Bubble Sci. Eng. Technol.* **1**, 31–39.
- Reznik, N., Williams, R., and Burns, P. N. (2011). "Investigation of vaporized submicron perfluorocarbon droplets as an ultrasound contrast agent," *Ultrasound Med. Biol.* **37**, 1271–1279.
- Sarkar, K., Katiyar, A., and Jain, P. (2009). "Growth and dissolution of an encapsulated contrast microbubble," *Ultrasound Med. Biol.* **35**, 1385–1396.
- Sarkar, K., and Prosperetti, A. (1994). "Coherent and incoherent-scattering by oceanic bubbles," *J. Acoust. Soc. Am.* **96**, 332–341.
- Sarkar, K., Shi, W. T., Chatterjee, D., and Forsberg, F. (2005). "Characterization of ultrasound contrast microbubbles using in vitro experiments and viscous and viscoelastic interface models for encapsulation," *J. Acoust. Soc. Am.* **118**, 539–550.
- Schad, K. C., and Hynynen, K. (2010). "In vitro characterization of perfluorocarbon droplets for focused ultrasound therapy," *Phys. Med. Biol.* **55**, 4933–4947.
- Sheeran, P. S., Matsunaga, T. O., and Dayton, P. A. (2013). "Phase-transition thresholds and vaporization phenomena for ultrasound phase-change nanoemulsions assessed via high-speed optical microscopy," *Phys. Med. Biol.* **58**, 4513–4534.
- Sheeran, P. S., Matsunaga, T. O., and Dayton, P. A. (2014). "Phase change events of volatile liquid perfluorocarbon contrast agents produce unique acoustic signatures," *Phys. Med. Biol.* **59**, 379–401.
- Sheeran, P. S., Wong, V. P., Luois, S., McFarland, R. J., Ross, W. D., Feingold, S., Matsunaga, T. O., and Dayton, P. A. (2011). "Decafluorobutane as a phase-change contrast agent for low-energy extravascular ultrasonic imaging," *Ultrasound Med. Biol.* **37**, 1518–1530.
- Shpak, O., Verweij, M., Vos, H. J., de Jong, N., Lohse, D., and Versluis, M. (2014). "Acoustic droplet vaporization is initiated by superharmonic focusing," *Proc. Natl. Acad. Sci.* **111**, 1697–1702.
- Strohm, E. M., and Kolios, M. C. (2011). "Sound velocity and attenuation measurements of perfluorocarbon liquids using photoacoustic methods," in *Proceedings of the 2011 IEEE International Ultrasonics Symposium (IUS)*, October 18–21, Orlando, FL, pp. 2368–2371.
- Vlaisavljevich, E., Aydin, O., Yuksel Durmaz, Y., Lin, K. W., Fowlkes, B., ElSayed, M., and Xu, Z. (2015). "Effects of ultrasound frequency on nanodroplet-mediated histotripsy," *Ultrasound Med. Biol.* **41**, 2135–2147.
- Williams, R., Wright, C., Cherin, E., Reznik, N., Lee, M., Gorelikov, I., Foster, F. S., Matsuura, N., and Burns, P. N. (2013). "Characterization of submicron phase-change perfluorocarbon droplets for extravascular ultrasound imaging of cancer," *Ultrasound Med. Biol.* **39**, 475–489.
- Zhang, P., Kopechek, J. A., and Porter, T. M. (2013). "The impact of vaporized nanoemulsions on ultrasound-mediated ablation," *J. Therap. Ultrasound* **1**, 2.
- Zhang, P., and Porter, T. (2010). "An in vitro study of a phase-shift nanoemulsion: A potential nucleation agent for bubble-enhanced HIFU tumor ablation," *Ultrasound Med. Biol.* **36**, 1856–1866.